buildings

MDPI

Article

Influence of Buried Pipeline Leakage on the Development of Cavities in the Subgrade

Xianghua Chen [1], Wenxin Chen [2], Liyuan Zhao [2] and Yekai Chen [2,*]

1 Guangzhou Traffic Design and Research Institute Co., Ltd., Guangzhou 510430, China
2 School of Civil Engineering and Transportation, South China University of Technology, Guangzhou 510641, China
* Correspondence: cheops@scut.edu.cn; Tel.: +86-133-2281-1833

Abstract: The rapid pace of urbanization has led to an increasing frequency of road collapses, posing a significant threat to urban traffic safety. Underground pipeline leakage stands out as the primary cause of such collapses. This paper presents a macroscopic analysis of the subgrade seepage erosion process caused by pipeline leakage. Model tests were conducted to investigate the formation mechanism and explore the influence of water level, water flow rate, and soil type. The study revealed that the subgrade seepage erosion caused by pipeline leakage undergoes four distinct stages: infiltration, slow erosion, rapid erosion, and erosion convergence. Soil erosion shares similarities with sand erosion in its developmental process. The water level plays a pivotal role in determining the shape and size of the eroded area caused by sand seepage erosion. The size of the erosion cavities formed during the soil seepage erosion increased along with the increase in the water flow rate. The size of the erosion cavity increased by up to 55.7% when the flow rate was increased by three times. In addition, clay soils do not undergo significant erosional damage but do produce significant settlement. The soil erosion process caused by underground leakages in pipelines was investigated using model tests in this study, which provided valuable information for researchers performing an in-depth analysis of the mechanism of roadbed cavities generated by urban underground pipeline leakage, which is critical for safeguarding people's travel safety and decreasing social and economic losses.

Keywords: road collapse; pipeline leakage; seepage erosion; model tests

Citation: Chen, X.; Chen, W.; Zhao, L.; Chen, Y. Influence of Buried Pipeline Leakage on the Development of Cavities in the Subgrade. *Buildings* **2023**, *13*, 1848. https://doi.org/10.3390/buildings13071848

Academic Editor: Salvatore Antonio Biancardo

Received: 28 June 2023
Revised: 14 July 2023
Accepted: 17 July 2023
Published: 21 July 2023

1. Introduction

The continuous development of urbanization has led to an increasing population density in cities, resulting in increased demand for urban resource development. To fulfill operational demands, underground engineering construction, recurrent building of underground pipeline networks, and subsurface water extraction operations have increased significantly [1–4]. Unfortunately, the frequency of urban road collapse accidents has increased, posing a severe threat to urban traffic safety. These accidents have resulted in major car accidents and significant loss of life in several circumstances [5–11].

According to research, underground pipeline leakage is the primary cause of urban road collapse accidents [12–17]. Groundwater seeps into the soil near the leaking pipeline, gradually eroding it and creating underground caves. If the soil above the caves is unable to support the weight above it, a sudden collapse occurs, resulting in road collapse accidents [18,19]. To investigate the damage pattern of soil seepage erosion, He et al. [20] proposed two modes, namely, the "cylindrical collapse mode" and the "funnel-shaped collapse mode", to explain the destructive modes of seepage erosion in underground cavity development. Liu et al. [21–23] investigated ground subsidence in water-rich sand layers caused by buried pipeline damage. The study identified three distinct modes of soil seepage erosion caused by pipeline damage: the first mode involves sudden water breakthrough without subsequent settlement; the second mode entails the formation of soil arches leading to settlement; and the third mode involves sand collapse accompanied by settlement.

Wang et al. [24] conducted model tests and identified two distinct failure patterns in sandy soil. The first pattern involves the development of hidden underground cavities with multiple arch formations during cavity evolution, while the second pattern involves surface cracking that results in the growth of an inverted triangle-shaped collapsed area.

Furthermore, numerous studies have been conducted to investigate the process of seepage erosion and the formation of underground cavities, as well as the various factors that influence them. These studies have employed model experiments to investigate issues such as soil loss, the progression of eroded cavities, and ground subsidence under varying conditions. Several researchers [25–28] discovered that the particle size distribution of the soil has a significant impact on seepage erosion, with smaller particles being more susceptible. Using a laboratory model test, Saton et al. [29] looked at how buried buildings affected internal erosion brought on by sewage breaches. The findings indicated that seepage erosion changes its path when a new pipeline is built close to the previous erosion channel. Karoui et al. [30] utilized laboratory modeling tests and revealed that the direction of groundwater flow, the hydraulic gradient around the seepage point, and the strength of the ground's support are the main factors that dominate the mechanism of ground subsidence. These factors can significantly affect ground deformation, the direction of cavity expansion, the rate of settlement development, and the rate of collapse. Kwak et al. [31] investigated the impact of different rainfall intensities and hydraulic gradients on groundwater infiltration and soil erosion. The results showed that rainfall intensity had a significant effect on surface deformation, whereas an increase in hydraulic gradient increased cavity size. Haibat et al. [32] identified soil type as the primary contributor to ground subsidence and proposed a regression model to forecast and manage ground subsidence risk. Basim et al. [33] conducted experiments to quantify soil erosion under a variety of conditions, including varying pipeline damage sizes, variations in soil particle gradations, varying water levels in the sand, and the number of water flow cycles. Based on the results, the researchers developed a dimensionless model that can predict the rate of localized soil erosion caused by pipeline leakage.

In conclusion, current research on road collapse caused by underground pipeline leakage has yielded significant findings; however, several critical issues require further investigation. The current understanding of the mechanism underlying subgrade collapse caused by underground pipeline leakage is inadequate, and the precise triggering mechanism remains ambiguous. As a result, this study conducted model tests to comprehensively analyze the soil erosion process caused by underground pipeline leakage. It investigated the effects of three factors on roadbed seepage erosion: water level, water flow rate, and soil type. The study offers valuable information for researchers performing an in-depth analysis of the mechanism of roadbed cavities generated by urban underground pipeline leaking, which is critical for safeguarding people's travel safety and decreasing social and economic losses.

2. Test Methods

2.1. Test Apparatus

The model test setup is shown in Figure 1. This experimental setup consists of three major components: (1) A model box with a transparent plexiglass inner layer and an outer layer supported by a steel frame to ensure adequate rigidity. The inner layer has dimensions of 600 mm × 200 mm × 700 mm. The seepage pipeline is inserted through two holes on each side of the model box. It also has an adjustable-sized seepage hole on the bottom plate to aid in sand drainage. (2) The water supply system consists of a water tank and a seepage pipeline. The seepage pipeline, which has an internal diameter of 40 mm, is located on the model box's side panel, and includes a breakage port to simulate pipeline breakage within the subgrade. A water level control is installed in the water tank to maintain a constant water level, and a water stop valve is installed at the water outlet to regulate the water flow. (3) Data acquisition system: comprised of a camera and a sand collection box. The camera is mounted in front of the model box to record the entire sequence of pipeline leakage, seepage erosion, cavity formation, and soil collapse. The sand collection box is located in the model box's lower section to collect lost soil, which will then be dried and sieved to determine the dry mass.

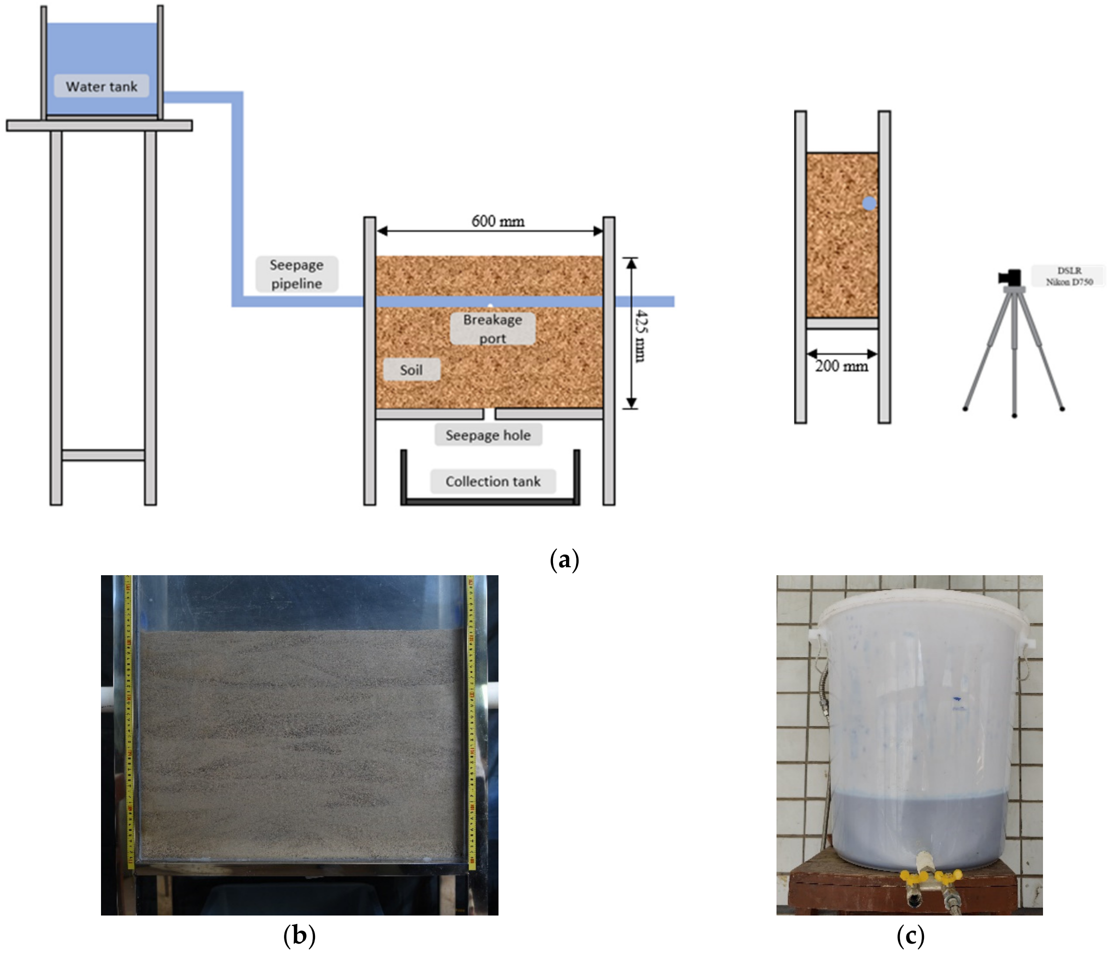

Figure 1. Model test apparatus. (**a**) Schematic diagram of the test setup. (**b**) Model box. (**c**) Water tank.

2.2. Test Materials

Several preliminary tests were performed before conducting formal seepage erosion tests. These tests included relative density, sieving, and normal head infiltration measurements. The sieving test was designed to determine the percentage of sand mass for different particle sizes. Following that, a particle gradation distribution curve was plotted and presented in Figure 2. Additionally, the sand's minimum and maximum porosity were measured using the measuring cylinder method and the vibratory hammer method, respectively. The test results revealed inhomogeneity and curvature coefficients of 4.36 and 1.32, along with maximum and minimum void ratios of 0.552 and 0.882, respectively. Moreover, the normal head permeability test was conducted, and it revealed the permeability coefficient of the sand to be 8.9×10^{-2} cm/s.

2.3. Test Conditions

Road collapses in urban areas caused by underground pipeline leakage are complex issues influenced by a variety of factors. When the groundwater level rises, for example, more water permeates the soil. As a result, the soil around the damaged or leaking pipeline loosens, making it more vulnerable to the effects of pipeline leakage. Furthermore, the flow rate of water within the pipeline can accelerate soil erosion, increasing the risk of road collapses. Different subgrade soils have distinct physical characteristics and stability properties. Certain subgrade soils, particularly those with loose structures, are highly susceptible to erosion caused by water seepage, increasing the risk of road failure. Therefore, this experiment considers three influencing factors: water level, water flow rate, and soil type. A total of 6 test groups were designed to investigate the effects of these factors on road collapses caused by underground pipeline leakage, following the principles of controlling variables. The test conditions are presented in Table 1.

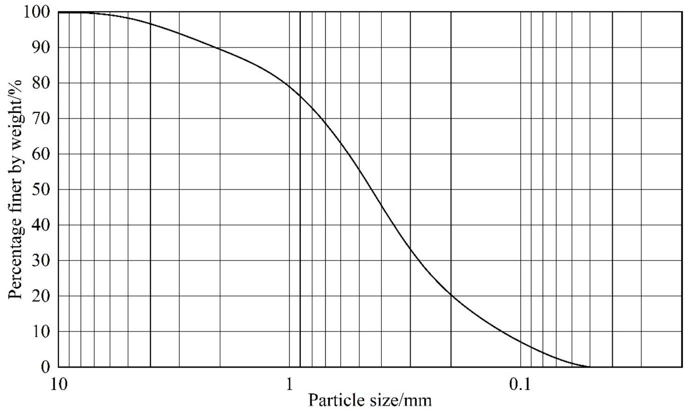

Figure 2. Sand particle size distribution.

Table 1. Test conditions.

Test	Water Level *H* (mm)	Water Flow Rate *Q* (mL/s)	Soil Type
1	60	51	sand
2	140	51	sand
3	220	51	sand
4	60	34	sand
5	60	17	sand
6	60	51	clay soil

2.4. Test Procedure

Figure 3 illustrates the experimental flow. Before initiating the test, it is crucial to dry the sand, eliminate impurities, and thoroughly mix it to achieve homogeneity. Subsequently, the pipeline should be installed, the seepage hole below the model box should be blocked, and petroleum jelly should be applied to the inner wall surface of the model box to mitigate the frictional effect.

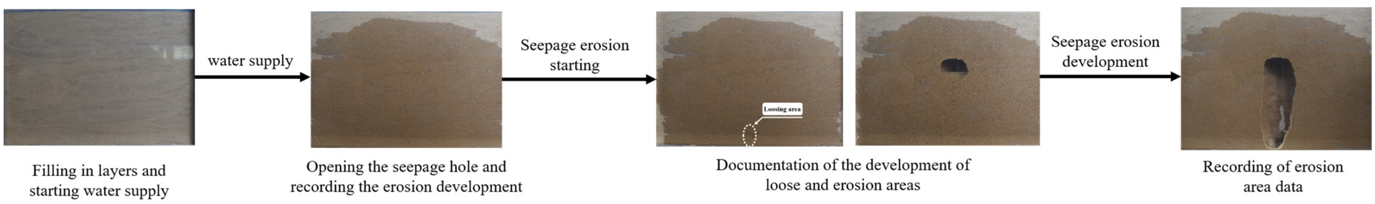

Figure 3. Test Flowchart.

The sand was layered and compacted for uniform distribution within the model box, ensuring proper compaction. Following that, the pipeline was inserted through the holes, and the layered compaction was resumed until the desired soil height was attained. To begin the test, open the water tank valve following the required water flow rate. The entire test was recorded to document the sand seepage erosion process. The sand that eroded into the sand collection box was dried after the test to determine the dry mass of the eroded soil. The sand inside the model box was then excavated systematically, and the box itself was thoroughly rinsed and dried in preparation for the next set of tests. Moreover, particle image velocimetry (PIV) was used to determine the velocity field distribution of sand particles in the test area.

3. Results and Discussion

3.1. The Sand Erosion around Defective Pipeline

Figure 4 illustrates the progression of seepage erosion resulting from pipeline defects observed in test 1, with other tests exhibiting comparable characteristics. As shown in Figure 5, the study used PIV analysis to determine the motion velocity of the sand particles in the 12 cm zones on each side of the model center to understand the behavior of particle movement. The cloud map indicates the direction and velocity of sand particles during the seepage erosion process.

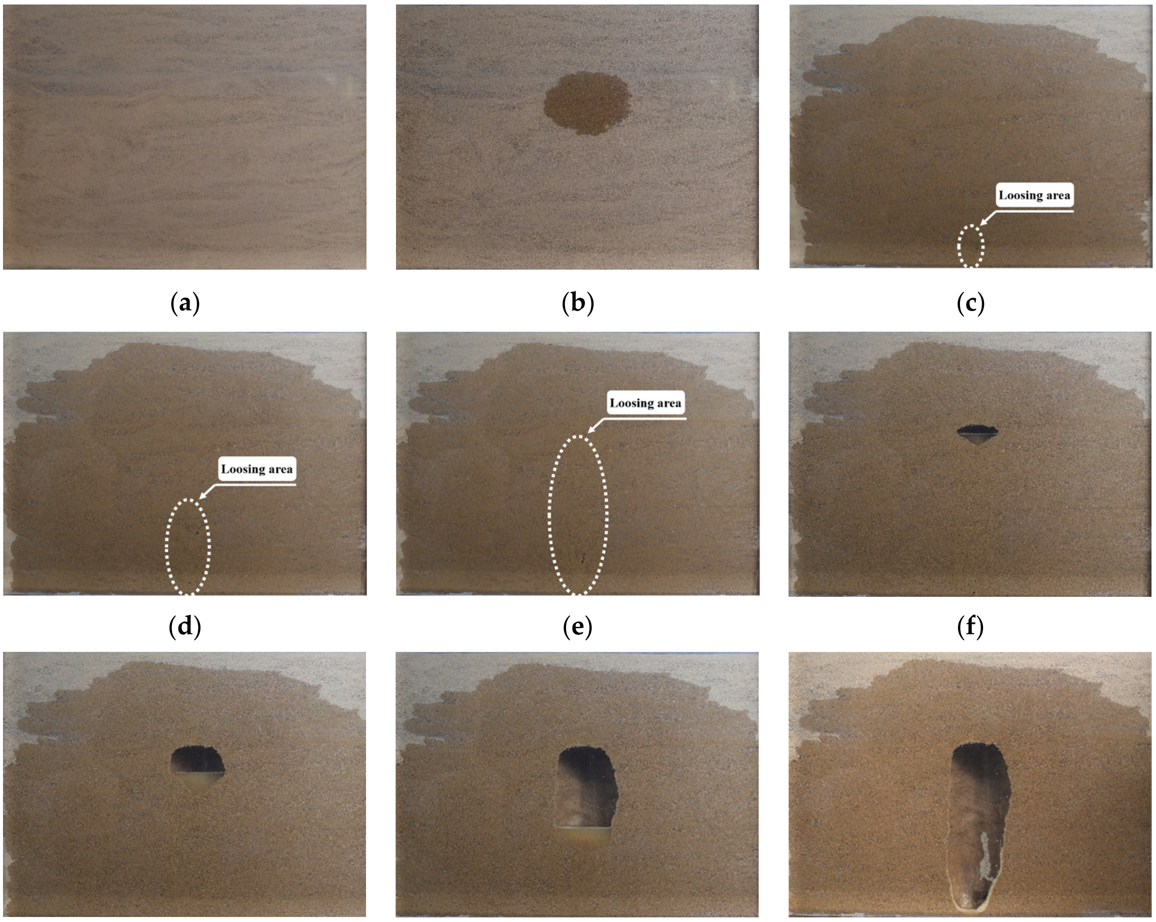

(**a**) (**b**) (**c**) (**d**) (**e**) (**f**) (**g**) (**h**) (**i**)

Figure 4. Erosion development in test 1. (**a**) t = 0 s. (**b**) t = 48 s. (**c**) t = 2380 s. (**d**) t = 2472 s. (**e**) t = 2556 s. (**f**) t = 2580 s. (**g**) t = 2640 s. (**h**) t = 2688 s. (**i**) t = 2736 s.

As the experiment began, a region of local infiltration was observed in the soil adjacent to the pipeline rupture, as illustrated in Figure 4b. The local wetted area consistently expanded as the seepage volume increased. The wetted region assumed an arched configuration, gradually ascending due to the impact of seepage flow force and ascending further through capillary action upon surpassing the height of the pipeline seepage opening. The infiltration boundary eventually reached stability after 1382 s. The matrix suction among the particles gradually decreased as the sand saturated, resulting in a significant decrease in the shear strength of the sandy soil within the saturated area. The flowing water transports fine particles that seep out and induce gradual relaxation of the sand. Consequently, the sand adjacent to the seepage hole is the first to experience loss, leading to the formation of an elliptical area of loosening close to the hole at 2380 s (Figure 4c).

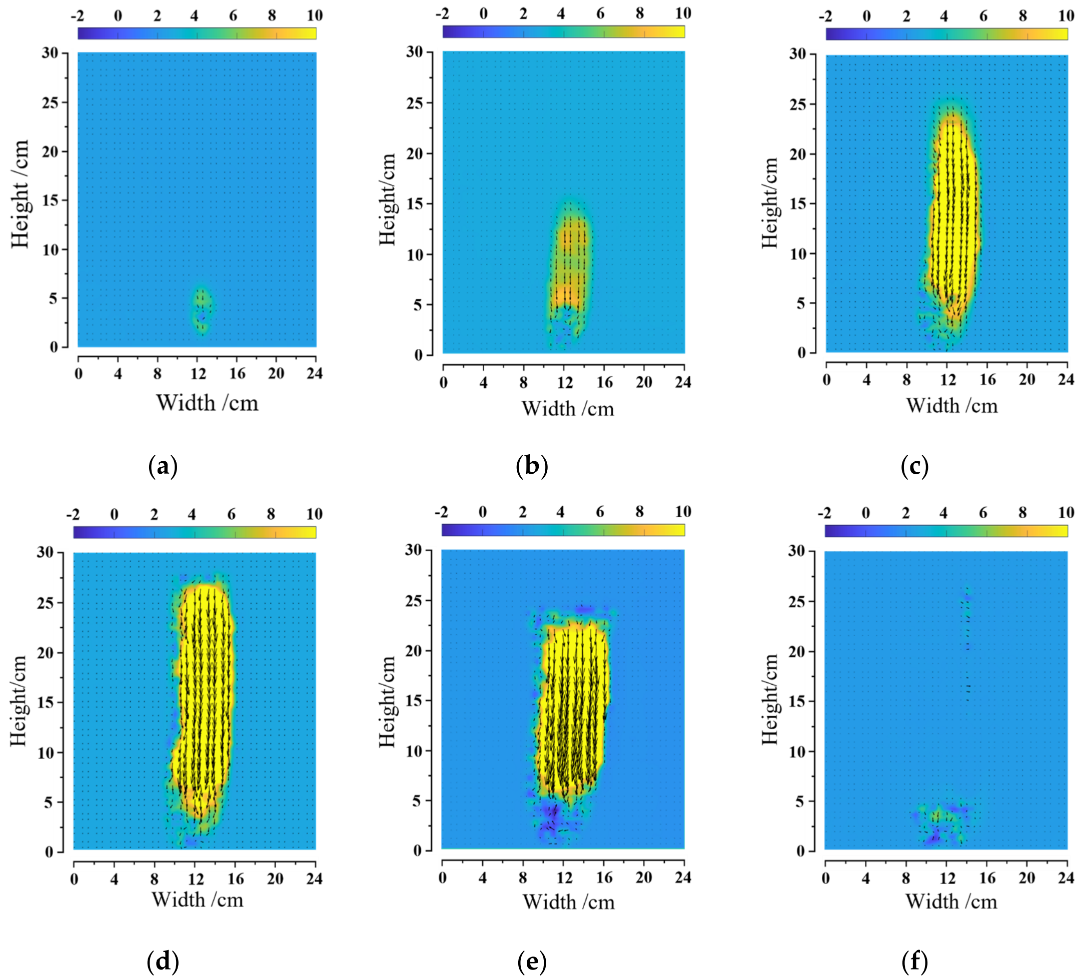

Figure 5. Velocity and contour of sand movement in Test 1 (velocity unit: mm/s): (**a**) t = 2380 s; (**b**) t = 2472 s; (**c**) t = 2556 s; (**d**) t = 2580 s; (**e**) t = 2640 s; (**f**) t = 2712 s.

As time progressed, the sand above this region gradually descended due to diminished support from the underlying sand, resulting in an elliptical loosening area expanding in an upward vertical direction (Figure 4d,e). At 2580 s, a small hidden cavity formed beneath the seepage hole due to sand loss (Figure 4f). The cavity formation reduced the seepage path length, increasing both the fluid and sand flow rates (Figure 4g,h). As a result of the combined forces of gravity and seepage, the erosion cavity rapidly expanded downward, eventually leading to the formation of a stable cavity at 2736 s (Figure 4i). The erosion cavity's critical damage area was determined to be close to the cylindrical damage, with a maximum width of 101 mm horizontally and 276 mm vertically.

Figure 6 illustrates the temporal evolution of the dry mass of eroded soil. Three inflection points can be observed in the figure. As a result, soil erosion can be divided into four stages: infiltration, slow erosion, rapid erosion, and erosion convergence.

In the infiltration stage, the localized infiltration area expanded while the water level increased. The flow rate was low during this stage, leading to a gradual rise in total seepage volume. The localized infiltration area gradually expanded outward from the breakage port, and it required a significant duration for the soil to attain a "fluidized state", signifying the formation of the loosening area. The first inflection point, observed at t = 2380 s, indicates the start of the slow erosion stage. The loosening area formed and gradually spread upward. The soil near the seepage hole underwent minor loss, while the soil above continually replenished and migrated downward due to the combined effects of gravity and seepage forces. Eventually, a small cavity developed at t = 2580 s. Following the formation of the cavity, there was an increase in the seepage flow rate and seepage force, while the seepage path shortened. This signifies the initiation of the rapid erosion stage, characterized by the rapid expansion of the cavity and substantial soil loss accompanied by the water flow. The erosion convergence stage began with the third inflection point at t = 2710 s. The dry mass of eroded soil reached a stabilization point, indicating that soil erosion development had stopped and a stable erosion cavity had formed.

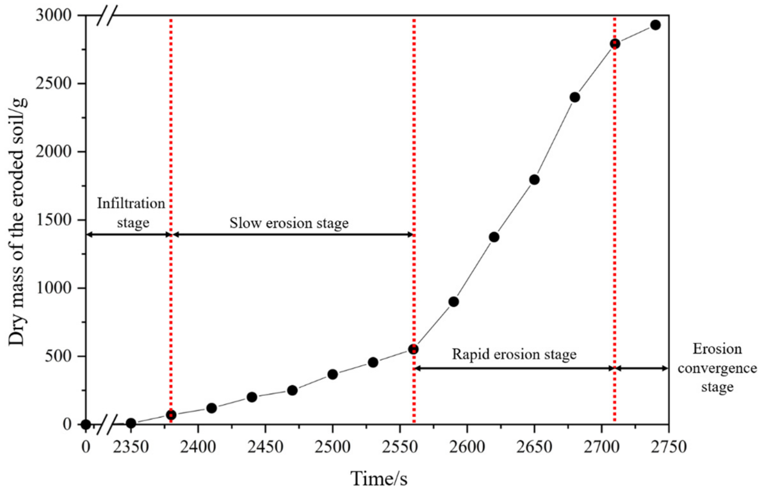

Figure 6. The development pattern of dry mass of eroded soil with time.

3.2. The Effect of Water Level

The higher the water level, the later the seepage hole was opened. The process of sand erosion changed as the water level rose. Figure 7 depicts the sand erosion process in test 3, while test 2 demonstrates comparable characteristics. Similar to Section 3.1, a PIV analysis was performed for a region 12 cm on either side of the model's center. The results were acquired and are shown in Figure 8 as the sand particles' velocity of movement. The direction and speed of sand particles during the seepage erosion process are shown on the cloud map.

Test 3 exhibits a larger ellipsoidal loose area during the development of seepage erosion due to the higher water level. At t = 780 s, seepage erosion started to occur in the sand. With the development of seepage erosion, the loosening area gradually expanded and the sand movement velocity increased. At t = 812 s, a smaller cavity forming an inverted triangle formed beneath the leakage port. Following that, the speed of sand movement increased further, and the sand within the loosening area traveled rapidly outward toward the seepage hole, eventually forming a large erosion cavity. As the water level rose, the water content inside the model box increased, allowing the water flow to fill the whole cavity. As a result, the resulting cavity was larger.

A comparison and analysis of erosion states under different water level conditions, depicted in Figure 9, reveals two distinct differences. To begin, the size of the sand infiltration surface varied. As the water level rose, so did the critical infiltration line height and the area of the infiltration surface. The infiltration line height extended to the top surface of the sand at a water level of 220 mm, fully wetting the entire sand surface. Second, the final erosion cavity's size varied. A higher water level resulted in greater erosion width and height, resulting in a larger erosion cavity.

The destructive morphology underwent corresponding changes. At a water level of 60 mm, the final destructive morphology took on an approximately cylindrical shape, exhibiting a rectangular shape on the surface of the model box wall. However, at water levels of 140 mm and 220 mm, the final destructive morphology of the soil in the water manifested as an inverted cone shape. This is because a higher water level causes more water dispersion in the soil, which causes more soil disturbance. The soil begins to flow, causing the saturated area of the sand to expand. As a result, the loosened area expands.

Furthermore, a higher water level puts more pressure on the seepage, causing more sand to enter the erosion outlet. As a result, as the water level rises, so does the size of the resulting erosion cavity.

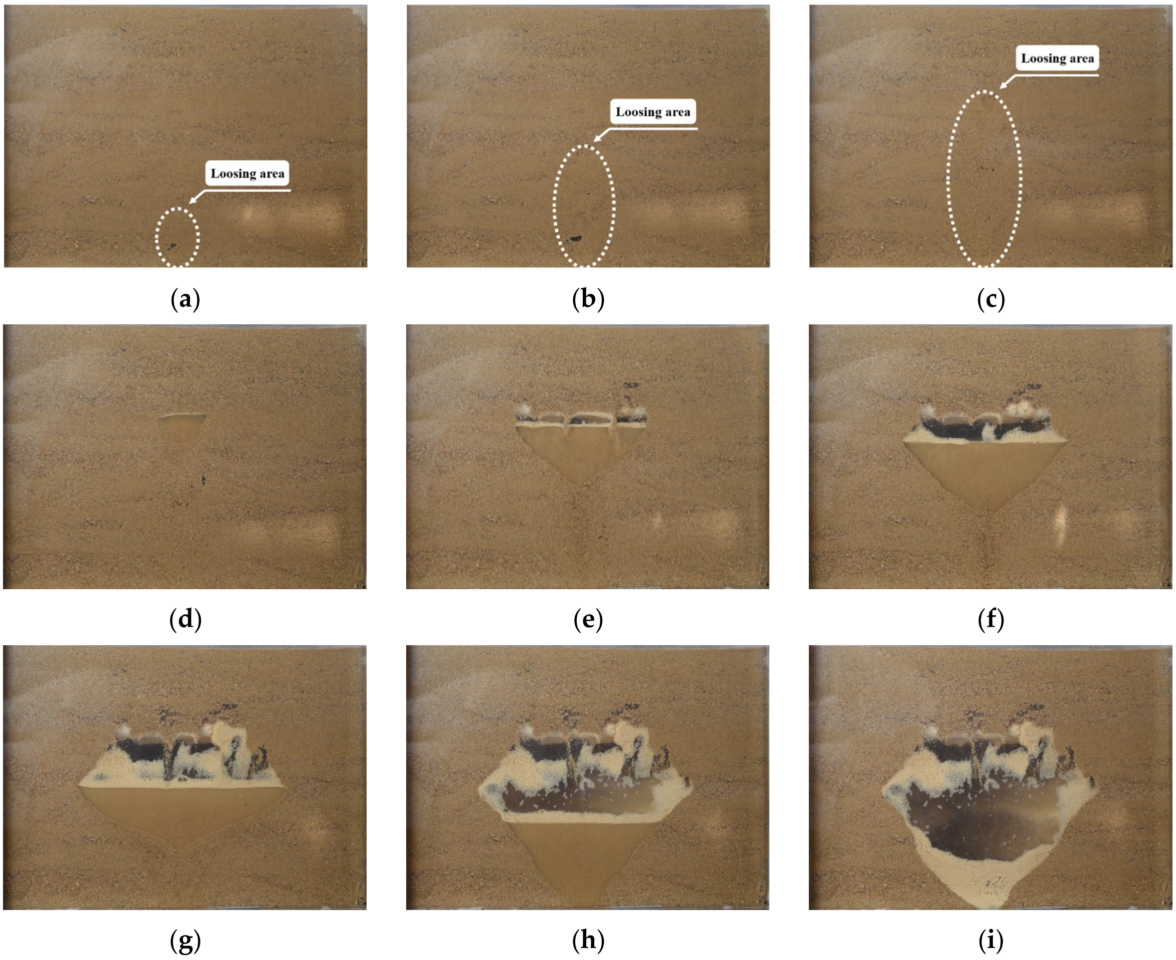

Figure 7. Erosion development in test 3: (**a**) t = 780 s; (**b**) t = 794 s; (**c**) t = 800 s; (**d**) t = 812 s; (**e**) t = 826 s; (**f**) t = 836 s; (**g**) t = 886 s; (**h**) t = 910 s; (**i**) t = 944 s.

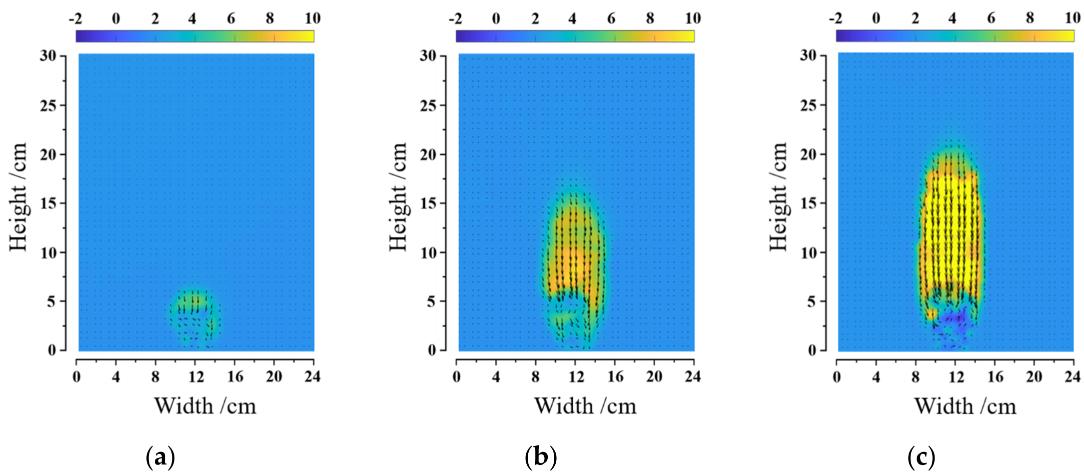

Figure 8. *Cont.*

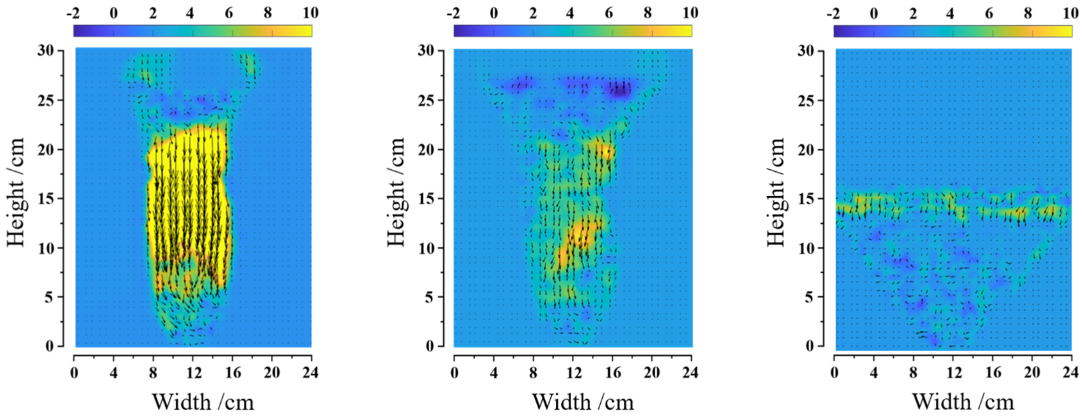

(**d**) (**e**) (**f**)

Figure 8. Velocity and contour of sand movement in Test 3 (velocity unit: mm/s): (**a**) t = 780 s; (**b**) t = 794 s; (**c**) t = 800 s; (**d**) t = 810 s; (**e**) t = 822 s; (**f**) t = 910 s.

According to the data in Table 2, as the water level rose to 60 mm, 140 mm, and 220 mm, the formation time of the infiltration line decreased to 23 min, 18 min, and 12 min, respectively, while the total slumping time decreased to 46 min, 28 min, and 16 min. These findings show that, as water levels rose, the erosion rate of sand increased. The rate of seepage erosion increased with the increase in water level. The duration of seepage erosion decreased from 46 min to 16 min when the water level was raised from 60 mm to 180 mm, a change of 65%. Furthermore, higher water levels cause more sand erosion. As the water level rose to 60 mm, 140 mm, and 220 mm, the dry mass of eroded soil increased from 2.93 kg to 13.59 kg, an increase of 364%; the erosion cavity cross-sectional area increased from 19,822.7 mm^2 to 69,038.1 mm^2, an increase of 248%; and the maximum width of the cavity increased from 109 mm to 351 mm, an increase of 222%. This is due to increased water dispersal in the soil as the water level rose. The greater infiltration force generated by the increased water level caused more soil disturbance, resulting in an expansion of the infiltration range and, as a result, increased sand erosion.

Table 2. Erosion area in different water level.

	Results	H = 60 mm	H = 140 mm	H = 220 mm
1	Infiltration surface formation time/min	23	18	12
2	Infiltration line height/mm	409	415	422.5
3	Seepage erosion time/min	46	29	16
4	Dry mass of eroded soil/kg	2.93	10.02	13.59
5	Erosion cavity cross-sectional area/mm^2	19,822.7	54,853.6	69,038.1
6	Maximum width of cavity/mm	109	275	351
7	Vertical depth of cavity/mm	268	298	332

3.3. The Effect of Water Flow Rate

The model experiments conducted have shown a consistent erosion development process of sandy soil under different water flow rates, resulting in final failure modes approximating an elliptical shape (Figure 10). This suggests that variations in water flow rate do not significantly impact the process of soil erosion caused by pipeline leakage or the final damage pattern. However, when the water flow rate increased, so did the size of the erosion cavities generated during soil seepage erosion. At a flow rate of Q = 17 mL/s, the breadth of the erosion cavity was 70 mm, whereas the biggest erosion cavity was 109 mm at a flow rate of 51 mL/s. When the flow rate was increased three times, the size of the erosion cavity increased by up to 55.7%.

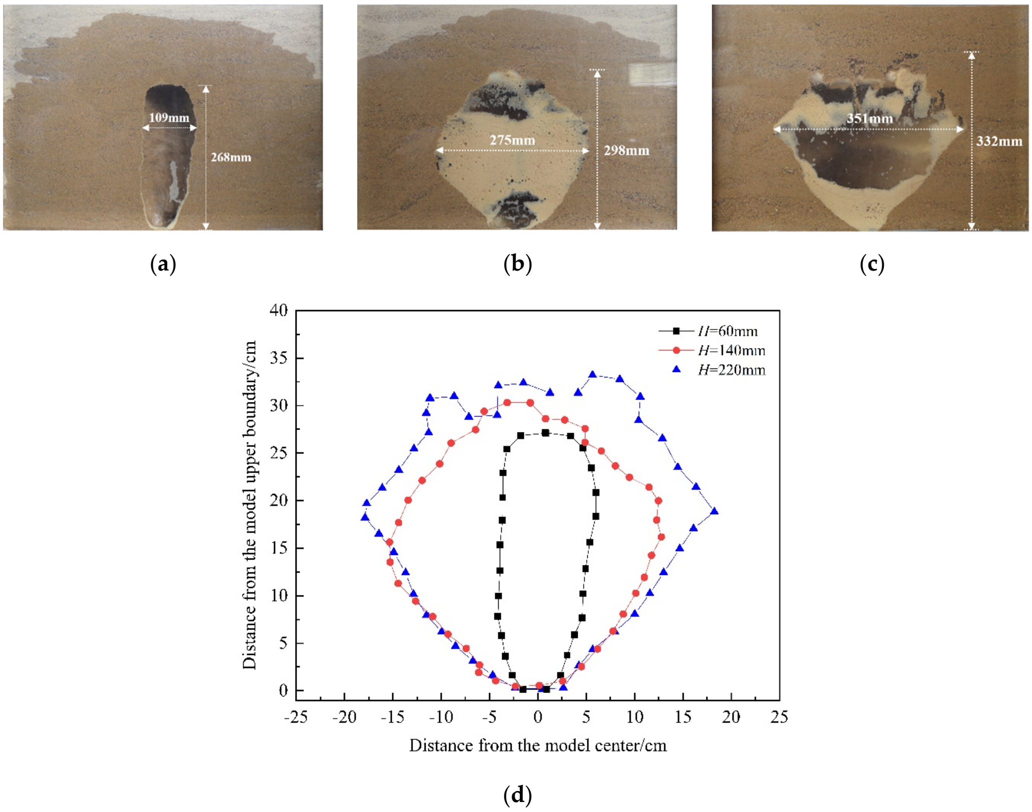

Figure 9. Erosion areas in different water levels: (**a**) H = 60 mm; (**b**) H = 140 mm; (**c**) H = 220 mm; (**d**) folded map of erosion area.

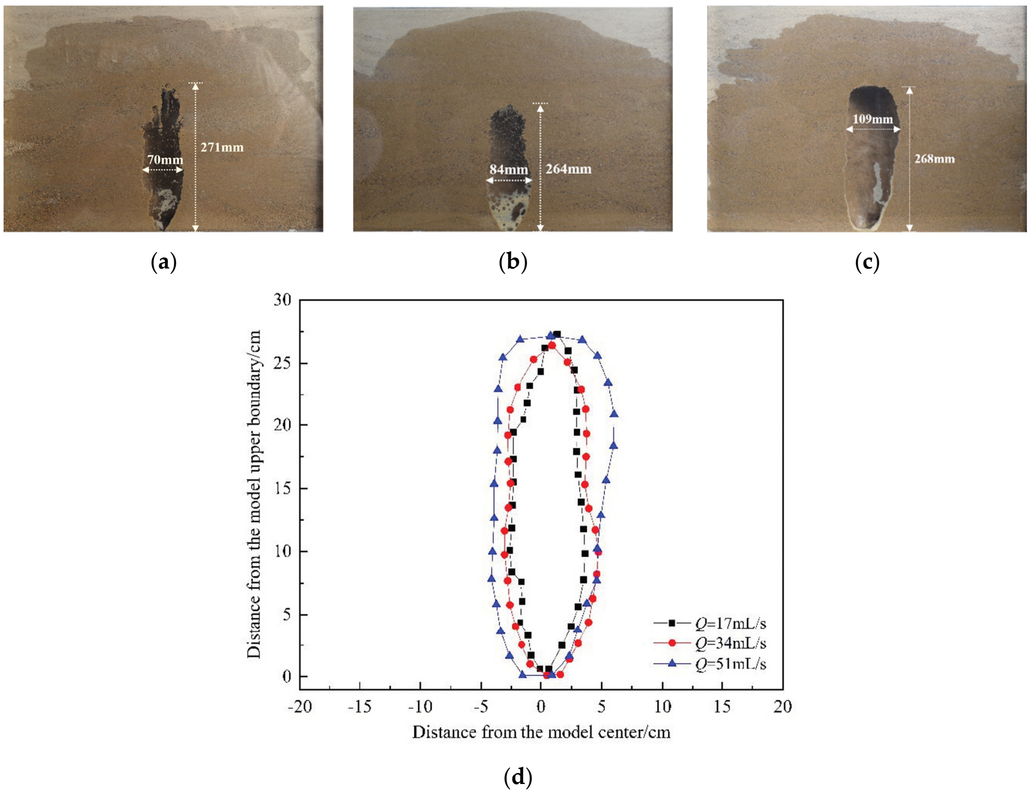

Figure 10. Erosion areas at different water flow rates: (**a**) Q = 17 mL/s; (**b**) Q = 34 mL/s; (**c**) Q = 51 mL/s; (**d**) folded map of erosion area.

Table 3 illustrates the results of soil seepage erosion in various water flow rate circumstances. The creation of the infiltrated surface took 21 min, 24 min, and 23 min for water flow rates of 17 mL/s, 34 min, and 51 min, respectively; whereas, the period from the start of the experiment to the formation of the final latent cavity was 45 min, 47 min, and 46 min. These observations indicate that variations in the water flow rate have a negligible impact on the erosion rate. However, the damage area created by the soil during seepage erosion increased with the increase in water flow rate. When the water flow rate increased from 17 mL/s to 51 mL/s, the dry mass of eroded soil increased from 2.41 kg to 2.93 kg, an increase of 22%; the erosion cavity cross-sectional area increased from 14,141.7 mm^2 to 19,822.7 mm^2, an increase of 40%; and the maximum width of the cavity increased from 70 mm to 109 mm, an increase of 55.7%. With an increase in water flow rate, there was an expansion in the extent of the erosion area. This can be attributed to the higher volume of water seeping through the leakage point, leading to an expansion of the saturated area in the sand and resulting in a larger erosion area.

Table 3. Erosion area in different water flow rate.

	Results	*Q* = 17 mL/s	*Q* = 34 mL/s	*Q* = 51 mL/s
1	Infiltration surface formation time/min	21	24	23
2	Infiltration line height/mm	402	412	409
3	Seepage erosion time/min	45	47	46
4	Dry mass of eroded soil/kg	2.41	2.59	2.93
5	Erosion cavity cross-sectional area/mm^2	14,141.7	16,961.4	19,822.7
6	Maximum width of cavity/mm	70	84	109
7	Vertical depth of cavity/mm	271	264	268

3.4. The Effect of Soil Type

Figure 11 illustrates the particle size distribution of the clay used in the tests. Figure 12 presents the results of the changes in the clay when the clay layer encountered a leakage from a buried pipeline. The water content of the clay near the pipeline crack grew significantly during the early part of the test, and the clay in this location began to settle. The water content of the clay layer below the pipeline steadily grew as the water seepage from the pipeline increased, the range in which the soil settled gradually expanded, and finally the surface of the soil layer settled. The clay layer's surface eventually experienced substantial settlement, with a maximum settlement value of 41 mm and the creation of visible fissures.

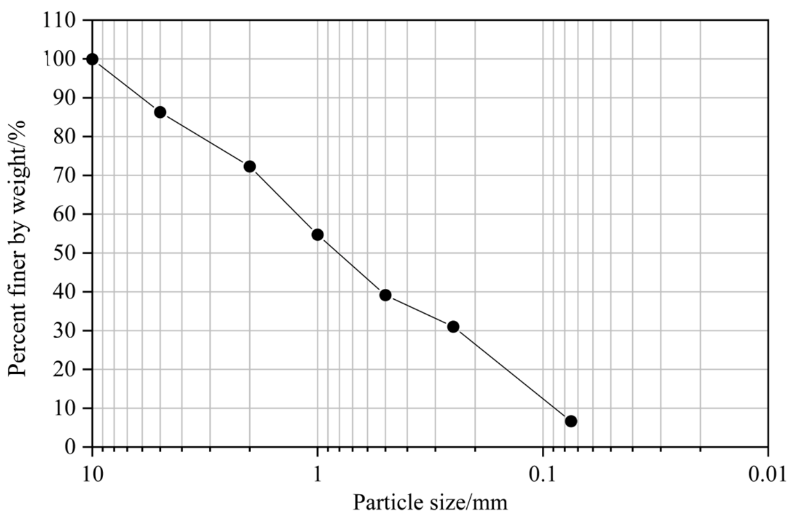

Figure 11. Particle size distribution of clay soil.

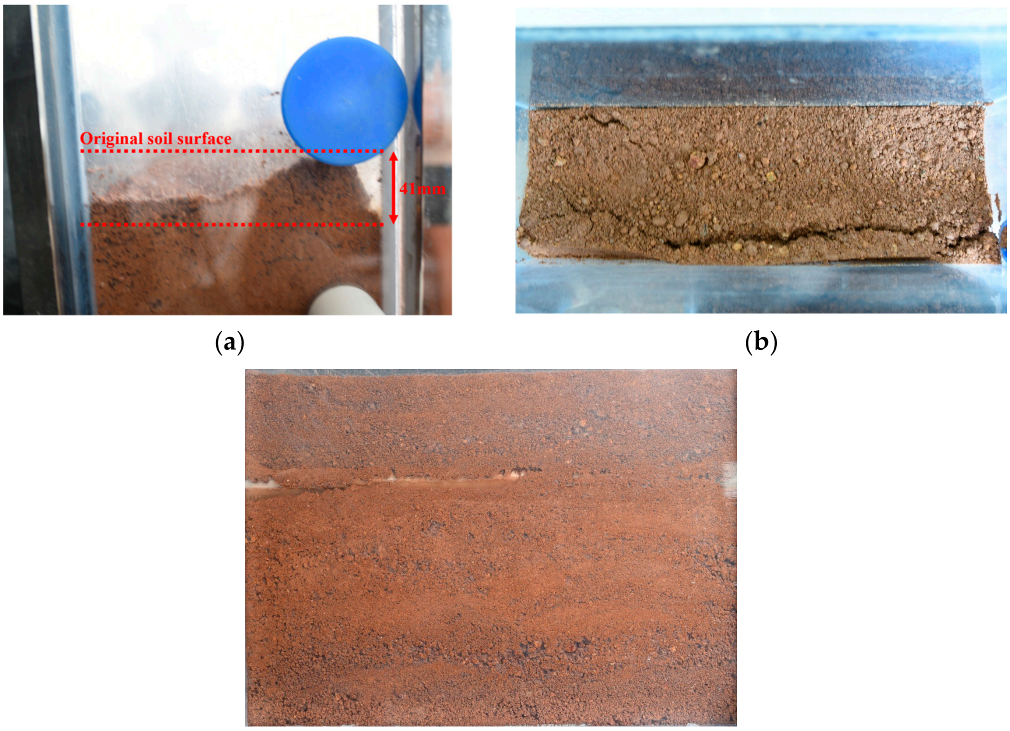

(**a**) (**b**) (**c**)

Figure 12. Final erosion state of clay soil: (**a**) surface settlement; (**b**) surface cracks; (**c**) surface of model box.

The test findings demonstrated that when the clay layer encountered pipeline leakage, there would be no evident soil seepage erosion or erosion zones in the soil layer, but rather obvious settlement on the soil layer's surface. Clay particles' inherent viscosity and plasticity allow them to deform rapidly during seepage erosion, resulting in soil subsidence and effective void filling.

4. Conclusions

This article addresses the issue of road collapse resulting from underground pipeline leakage. A self-designed indoor model test apparatus was employed to comprehensively analyze the macroscopic process of subgrade soil seepage erosion, exploring the effects of water level, water flow rate, and soil type on soil erosion. The primary findings are summarized as follows:

(1) The seepage erosion process can be divided into four stages based on the progression of sand erosion: infiltration, slow erosion, rapid erosion, and erosion convergence.
(2) The water level plays a vital role in determining the shape and size of the eroded area resulting from sand seepage erosion. With increasing water levels, the shape of the eroded area underwent a gradual transition from a rectangle to an inverted cone, accompanied by an expansion in its extent.
(3) As the water flow rate increased, the size of the erosion cavities generated during soil seepage erosion increased. When the flow rate was increased three times, the size of the erosion cavity increased by up to 55.7%.
(4) In the case of a pipeline breach in a clay layer, the soil layer's surface will experience significant settlement, but there won't be any significant seepage erosion.

5. Recommendations for Future Studies

In this study, the effects of water level, water flow rate, and soil type on soil seepage erosion were investigated through laboratory model tests. The factors influencing soil seepage erosion of subgrade caused by buried pipeline leakage are various, and the research on soil seepage erosion caused by pipeline leakage still needs to be further supplemented and improved. The main contents are as follows:

Subgrade soils are subjected to the load effects of the vehicles traveling above and the disturbance of the surrounding construction in real-life situations. Therefore, the development process of soil seepage erosion under the combined effects of pipeline seepage and loads can be investigated in the future.

On actual roads, when soil seepage erosion develops further, it can cause disasters such as roadway collapse. Future research could focus on the effects of soil seepage erosion on road collapse and travel safety.

The formation of hidden cavities in the subgrade seriously affects the safety of roads. The formation of hidden voids in the roadbed seriously affects the safety of road use. The prevention and control measures needed to delay the development of subgrade cavities and prevent road collapse will be the focus of the next phase of research.

Author Contributions: Conceptualization, X.C. and Y.C.; Methodology, X.C., W.C. and Y.C.; Investigation, W.C. and L.Z.; Writing—original draft, W.C. and L.Z.; Writing—review & editing, X.C.; Supervision, Y.C. All authors have read and agreed to the published version of the manuscript.

Funding: This research was funded by the National Natural Science Foundation of China (Grant No. 51908139), the project of Zhejiang Provincial Construction Department (Grant No. 2022K073), and the project of Zhejiang Provincial Science and Technology Department (Grant No. 2022C03180).

Institutional Review Board Statement: Not applicable.

Informed Consent Statement: Not applicable.

Data Availability Statement: The data presented in this study are available on request from the corresponding author.

Acknowledgments: The authors would like to thank the technicians in the road laboratories of South China University of Technology for the technical support and assistance in experimental activities.

Conflicts of Interest: The authors declare that they have no known competing financial interest or personal relationship that could have appeared to influence the work reported in this paper.

References

1. Guo, S.; Zhang, T.; Zhang, Y.; Zhu, D.Z. An approximate solution for two-dimensional groundwater infiltration in sewer systems. *Water Sci. Technol.* **2013**, *67*, 347–352. [CrossRef] [PubMed]
2. Yuan, J.; Mao, W.; Hu, C.; Zheng, J.; Zheng, D.; Yang, Y. Leak detection and localization techniques in oil and gas pipeline: A bibliometric and systematic review. *Eng. Fail. Anal.* **2023**, *146*, 107060. [CrossRef]
3. Abbasi, A.; Khatibinia, M.; Jahangir, H.; Dos Santos, J.V.A.; Lopes, H.M.R. Shearography-Wavelet-Based Damage Detection Methodology for Aluminum Beams. *J. Rehabil. Civ. Eng.* **2023**, *11*, 22–43.
4. Wang, W.; Gao, Y. Pipeline leak detection method based on acoustic-pressure information fusion. *Measurement* **2023**, *212*, 112691. [CrossRef]
5. Galve, J.P.; Gutiérrez, F.; Guerrero, J.; Alonso, J.; Diego, I. Optimizing the application of geosynthetics to roads in sinkhole-prone areas on the basis of hazard models and cost-benefit analyses. *Geotext. Geomembr.* **2012**, *34*, 80–92. [CrossRef]
6. Wang, P. Application of ground penetrating radar in detection of underground diseases of side walk. *Bull. Surv. Mapp.* **2019**, 199–203.
7. Soleymani, A.; Jahangir, H.; Nehdi, M.L. Damage detection and monitoring in heritage masonry structures: Systematic review. *Constr. Build. Mater.* **2023**, *397*, 132402. [CrossRef]
8. Nasab, M.N.; Jahangir, H.; Hasani, H.; Majidi, M.-H.; Khorashadizadeh, S. Estimating the punching shear capacities of concrete slabs reinforced by steel and FRP rebars with ANN-Based GUI toolbox. *Structures* **2023**, *50*, 1204–1221. [CrossRef]
9. Li, X.; Chen, Y.; Zou, C.; Wu, J.; Shen, Z.; Chen, Y. Building coupling loss measurement and prediction due to train-induced vertical vibrations. *Soil Dyn. Earthq. Eng.* **2023**, *164*, 107644. [CrossRef]
10. Zou, C.; Moore, J.A.; Sanayei, M.; Tao, Z.; Wang, Y. Impedance model of train-induced vibration transmission across a transfer structure into an overtrack building in a metro depot. *J. Struct. Eng.* **2023**, *148*, 04022187. [CrossRef]
11. Li, X.; Chen, Y.; Zou, C.; Chen, Y. Train-induced vibration mitigation based on foundation improvement. *J. Build. Eng.* **2023**, *76*, 107106. [CrossRef]
12. Tohda, J.; Hachiya, M. Response and design of buried pipelines subjected to differential ground settlement. In Proceedings of the 16th International Conference on Soil Mechanics and Geotechnical Engineering, Osaka, Japan, 12–16 September 2005; pp. 1659–1662.

13. Zhong, S.Y.; Cong, B.R. The genetic mechanism and classification of urban ground collapses hazard. *J. Eng. Geol.* **2016**, *24*, 358–363.
14. Guo, L.F.; Chai, S.Q.; Dong, J.Y.; Xiao, Z.T.; Yu, Q.Z. A Statistical Analysis of Urban Road Collapse Accidents in China. *J. Eng. Manag.* **2020**, *34*, 49–54.
15. Hu, J.H.; Bai, Y.C.; Xu, H.Y. Analysis of reasons for urban road collapse and prevention and control countermeasures in recent decade of China. *Highway* **2016**, *61*, 130–135.
16. Shi, Q.H.; Wei, H.L.; Tan, F.; Zhou, J.W.; Zhu, J.H. Analyzing the characteristics and reason for the ground collapse hazard in Shenzhen. *Bull. Geol. Sci. Technol.* **2022**, *41*, 123–129.
17. Chen, Y.A.; Tang, R.; Fang, J.; Kong, F. Analysis on spatio-temporal law and causation of urban road collapse in China from 2014 to 2018. *Water Resour. Hydropower Eng.* **2020**, *51*, 108–116.
18. Zheng, T. Nonlinear Finite Element Study of Deteriorated Rigid Sewers Including the Influence of Erosion Voids. Master's Thesis, Department of Civil Engineering, Queen's University, Kingston, ON, Canada, 2007.
19. Balkaya, M.; Moore, I.D.; Sag Lamer, A. Study of non-uniform bedding due to voids under jointed PVC water distribution pipes. *Geotext. Geomembr.* **2012**, *34*, 39–50. [CrossRef]
20. He, Z.M.; Yang, Y.; Zeng, X.F.; Liu, S.Z. Response analysis of subgrade deformation in evolution of concealed soil cave. *J. Cent. South Univ. Sci. Technol.* **2018**, *49*, 3068–3076.
21. Liu, C.Y.; Chen, B.W.; Luo, H.L.; Ruan, J.C. Experimental study of seepage erosion induced by pipeline damage under full pipe flow condition. *Rock Soil Mech.* **2020**, *41*, 1–10.
22. Liu, C.Y.; Zhang, X.; Cheng, K.; Chen, B.W. Experimental study of settlement caused by water and sand inrush in underground engineering. *Rock Soil Mech.* **2019**, *40*, 843–851.
23. Liu, C.Y.; Chen, B.W.; Lin, W.; Luo, H.L. Prediction model for settlement caused by damage of underground pipelines and its experimental verification. *Chin. J. Geotech. Eng.* **2021**, *43*, 416–424.
24. Wang, Y.Z. *Study on the Mechanism of Sandy Soil Erosion into Cavities under Different Hydraulic Conditions*; Shandong Jianzhu University: Jinan, China, 2020.
25. Indiketiya, S.; Piratheepan, J.; Pathmanathan, R. Evaluation of defective sewer pipe–induced internal erosion and associated ground deformation using laboratory model test. *Can. Geotech. J.* **2017**, *54*, 1184–1195. [CrossRef]
26. Tang, Y.; David, Z.Z.; Dave, H.C. Experimental Study on Submerged Sand Erosion through a Slot on a Defective Pipe. *J. Hydraul. Eng.* **2017**, *143*, 04017026. [CrossRef]
27. Zhang, D.M.; Du, W.W.; Guo, C.P. Model tests on seepage erosion caused by pipeline damage in gap-grading sand. *Chin. J. Geotech. Eng.* **2017**, *40*, 429–438.
28. Zhang, D.M.; Wei-Wei, D.; Guo, C.P. Model Test of Seepage Erosion Around Defective Buried Pipelines. In *Proceedings of Geoshanghai 2018 International Conference: Multi-Physics Processes in Soil Mechanics and Advances in Geotechchnical Testing*; Springer: Singapore, 2018; pp. 261–270.
29. Sato, M.; Kuwano, R. Influence of location of subsurface structures on development of underground cavities induced by internal erosion. *Soils Found.* **2015**, *55*, 829–840. [CrossRef]
30. Karoui, T.; Jeong, S.Y.; Jeong, Y.H.; Kim, D.S. Experimental Study of Ground Subsidence Mechanism Caused by Sewer Pipe Cracks. *Appl. Sci.* **2018**, *8*, 679. [CrossRef]
31. Kwak, T.Y.; Woo, S.I.; Kim, J.; Chung, C.K. Model test assessment of the generation of underground cavities and ground cave-ins by damaged sewer pipes. *Soils Found.* **2019**, *59*, 586–600. [CrossRef]
32. Haibat, A.; Choi, J. Risk Prediction of Sinkhole Occurrence for Different Subsurface Soil Profiles due to Leakage from Underground Sewer and Water Pipelines. *Sustainability* **2020**, *12*, 310.
33. Nile, B.K.; Al-Baidhani, J.H.; Ghulam, A.N. A Dimensional Analysis of Local Sandy Soil Erosion Induced By Leaky Sewer Pipes. *IOP Conf. Ser. Mater. Sci. Eng.* **2020**, *928*, 22142. [CrossRef]